Sixth International Symposium on Turbulence and Shear Flow Phenomena
Seoul, Korea, 22-24 June 2009

TOWARDS LARGE-EDDY SIMULATIONS OF HIGH-REYNOLDS NUMBER TURBULENT BOUNDARY LAYERS

Philipp Schlatter, Qiang Li, Geert Brethouwer, Arne V. Johansson, Dan S. Henningson
Linné Flow Centre, KTH Mechanics
SE-100 44 Stockholm, Sweden
pschlatt@mech.kth.se

ABSTRACT

Well-resolved large-eddy simulations (LES) of a spatially developing turbulent boundary layer under zero pressure gradient up to comparably high Reynolds numbers ($Re_\theta = 4300$) are performed. The inflow is located at $Re_{\delta^*} = 450$ ($Re_\theta \approx 300$), a position where natural transition to turbulence can be expected. Results are validated and compared extensively to both numerical data sets (*e.g.* an on-going fully-resolved spatial direct numerical simulation (DNS) up to $Re_\theta = 2500$) and available experimental measurements, *e.g.* the ones obtained by Österlund *et al.* (1999). The goal is to provide the research community with reliable numerical data for high Reynolds-number wall-bounded turbulence, which can in turn be employed for further model development and validation, but also to contribute to the characterisation and understanding of wall turbulence.

The results obtained via LES show that good agreement with existing data, both numerically at lower Reynolds numbers and experimentally, can be obtained for both mean and fluctuating quantities. In addition, turbulence spectra characterising large-scale organisation in the flow have been obtained and compared to literature results with good agreement. In particular, the near-wall streaks scaling in inner units and the outer layer, large-scale structures can clearly be identified in both spanwise and temporal spectra. The present contribution focuses on presenting selected results, in an effort to validate the chosen simulation approach and to initiate further studies analysing the simulation data.

INTRODUCTION

The turbulent flow close to solid walls is a major topic in today's research in fluid dynamics. Although in nature or technical applications the walls are usually curved and the mean flow is seldomly exactly two-dimensional, the spatially developing, zero-pressure gradient turbulent boundary layer on a flat plate has emerged as an important canonical flow case for theoretical, numerical as well as experimental studies. In recent years, several careful experiments have been conducted. For instance, Österlund *et al.* (1999) performed extensive measurements of mean and fluctuating quantities in the MTL wind tunnel at KTH Stockholm using hot-wire and hot-film anemometry for Reynolds numbers Re_θ based on the momentum thickness θ and the free-stream velocity U_∞ ranging from 2530 to 27300 (including five measurement positions below $Re_\theta = 6000$). Partly based on these experimental data, Monkewitz *et al.* (2007) have recently presented various asymptotic results for high Reynolds numbers, including the mean velocity profile.

However, as opposed to turbulent channel and pipe flow, relatively few numerical results of direct or large-eddy simulations (DNS/LES) of turbulent boundary layers have been published for medium or high Reynolds numbers. Spalart's simulations (Spalart, 1988) using an innovative spatio-temporal approach provided valuable data at $Re_\theta = 300, 670, 1410$. A true spatial DNS has been performed by Komminaho and Skote (2002) up to $Re_\theta = 700$. Using a similar numerical method, but in a fairly short domain, $Re_\theta = 2240$ was reached by Khujadze and Oberlack (2004). The highest Reynolds number reached in DNS to date is the data reported by Ferrante and Elghobashi (2005) at $Re_\theta = 2900$, however obtained in a comparably short computational domain in which the turbulence, in particular the large-scale structures, may not be fully developed. Either the computational approaches were too different to the experiments or the Reynolds numbers were too low to make possible a robust comparison between all those simulations and experiments. For turbulent boundary layers, the Reynolds number $Re_\theta \approx 4300$ has to be considered at present high from a simulation point of view. Due to the difficulty of both simulation, but also of experiments at Reynolds numbers Re_θ on the order of a few thousand, there is a comparably large spread of the existing data in the literature, both for integral, mean and fluctuating turbulent quantities, see *e.g.* Honkan and Andreopoulos (1997). There is thus a need for accurate and reliable simulation data of spatially developing turbulent boundary layers with Re_θ to be compared to high-quality experimental results. To this end, the inflow in the numerical simulation should be positioned far enough upstream, *i.e.* comparable to where natural transition occurs, to ensure that the flow reaches a fully developed, undisturbed equilibrium state further downstream. However, as pointed out by Österlund *et al.* (1999), a clear overlap region can only be detected above $Re_\theta = 6000$, which is still very high for adequately resolved numerical simulations.

The aim of the present study is to perform and validate well-resolved spatial large-eddy simulations (LES) in an effort to obtain accurate and reliable data at higher Reynolds numbers. A snapshot of such a simulation is presented in Figure 1, with several relevant downstream positions indicated. The inflow is positioned at a low streamwise Reynolds number, $Re_{\delta^*} = 450$ based on the displacement thickness δ^* at the inlet. An exhaustive amount of statistics, *e.g.* one and two-point statistics, Reynolds-stress budgets and time series pertaining to turbulent quantities, are collected and evaluated.

NUMERICAL METHODOLOGY

The simulations are performed using a fully spectral method to solve the three-dimensional, time-dependent, incompressible Navier-Stokes equations (Chevalier *et al.*, 2007). In the wall-parallel directions, Fourier series with dealiasing are used, whereas the wall-normal direction is discretised with Chebyshev polynomials. Time is ad-

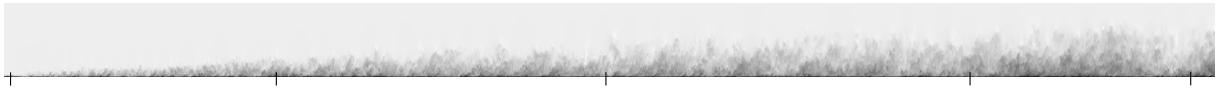

$Re_\theta = 300$ $Re_\theta = 1430$ $Re_\theta = 2558$ $Re_\theta = 3661$ $Re_\theta = 4303$

Figure 1: Instantaneous side view showing colour contours of the streamwise velocity component. The domain shown corresponds to the computational box for the present LES, reaching up to approximately $Re_\theta = 4400$. Note that only half of the domain extent in the wall-normal direction is shown, and the fringe region at the outflow is not included. The representation of the box is enlarged by a factor three in the wall-normal direction.

vanced with a standard mixed Crank-Nicolson/Runge-Kutta scheme. The periodic boundary conditions in the streamwise direction are combined with a spatially developing boundary layer by adding a "fringe region" at the end of the domain. In this region, the outflowing fluid is forced via a volume force to the laminar inflowing Blasius boundary-layer profile, located at $Re_{\delta_0^*} = 450$ based on the displacement thickness δ_0^* at the inlet. A low-amplitude trip force acting in the wall-normal direction is used to cause rapid laminar-turbulent transition shortly downstream of the inlet (see Figure 1). The spectral method provides excellent accuracy and dispersion properties as compared to low-order discretizations.

The computational domain is $x_L \times y_L \times z_L = 6000\delta_0^* \times 200\delta_0^* \times 240\delta_0^*$ with $4096 \times 385 \times 384$ spectral collocation points in the streamwise, wall-normal and spanwise directions, respectively. The height of the computational domain is chosen to be at least three times the largest 99%-boundary-layer thickness δ_{99}; in the spanwise direction an even larger domain has been chosen to ensure the correct development of large-scale structures scaling in outer units. The grid points are non-equidistantly distributed in the wall-normal direction, with at least 10 collocation points within the region $y^+ < 10$. The maximum grid spacing in viscous units is then $\Delta x^+ \times \Delta y^+_{\max} \times \Delta z^+ = 25.3 \times 14.2 \times 10.8$. The statistics are sampled over $\Delta t^+ \approx 20,000$ viscous time units. Owing to the high computational cost of the simulations, the numerical code is fully parallelised running on $\mathcal{O}(1000)$ processors.

Since the chosen resolution is not adequate for a direct numerical simulation, the unresolved quantities have to be treated via a subgrid-scale model. In the present case, the ADM-RT model (Schlatter *et al.*, 2004) has been employed, supplementing the governing equations with a dissipative term. This relaxation term is based on a high-order three-dimensional filter operation, and causes fluctuations close to the numerical cutoff to be damped. This additional dissipation regularises the flow solution, and allows to perform accurate simulations of both transitional and turbulent flows at reduced resolution, in particular for simulation methods based on spectral discretisation, see *e.g.* Schlatter *et al.* (2006). Note that the ADM-RT model converges by construction towards a DNS with increasing resolution.

AVERAGED RESULTS

As mentioned above, the inflow for the present simulation is located at $Re_{\delta^*} = 450$, roughly corresponding to $Re_\theta = 300$, which is low enough to ensure a physical flow development further downstream, see also Figure 1. Once a statistically stationary state has been reached, statistics are averaged over the spanwise direction z and time t.

The skin-friction coefficient c_f is shown in Figure 2. The transitional region at the beginning of the domain is clearly visible; based on c_f the LES is seen to reach a fully-developed state around $Re_\theta \approx 700$. Surprisingly, the comparably simple empirical correlation $c_f = 0.024 Re_\theta^{(-1/4)}$ (Kays and Crawford, 1993) provides an accurate fit to the present

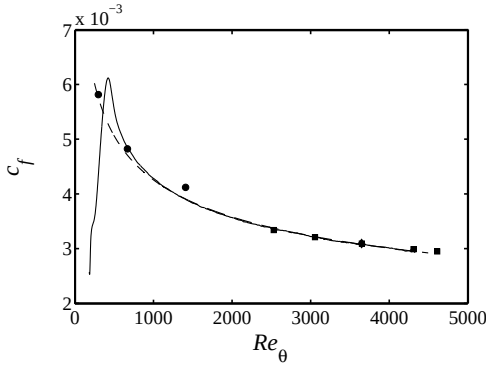

Figure 2: Skin-friction coefficient c_f as a function of Re_θ. ——— present LES, - - - - $c_f = 0.024 Re_\theta^{(-1/4)}$ (Kays and Crawford, 1993). • DNS by Spalart (1988), ■ experimental results by Österlund (1999).

LES data for the range of Reynolds numbers considered. In addition, the agreement with the experimental measurement points (Österlund, 1999) at in the range $Re_\theta = 2500$ to 4300 is very good. Recall that, experimentally the skin friction is obtained using an oil-film technique independent of the hot-wire velocity measurements. For comparison, the data points of the DNS by Spalart (1988) are also shown in Figure 2. The skin friction is overpredicted by approximately 5% at Spalart's highest $Re_\theta = 1410$. This might be a residual effect of the spatio-temporal approach employed for the simulation, which does not extent to higher Reynolds numbers.

Profiles of the mean velocity scaled in viscous units $U^+(y^+)$ obtained from the present LES are shown in Figure 3. For comparison, both DNS data from Spalart (1988) and experimental results by Österlund (1999) are shown as well. The similarity at the higher Reynolds numbers, *i.e.* $Re_\theta = 2500 - 4300$, is very satisfactory. However, there is a discrepancy between the present simulation data and that of Spalart at $Re_\theta = 1410$, which again might be attributed to the spatio-temporal simulation approach in the latter. In the near-wall region, all data collapse nicely on the linear relation $U^+ = y^+$ according to the asymptotic expansion for the viscous sublayer. The von Kármán coefficient κ used to indicate the logarithmic region $(1/\kappa)\log y^+ + B$ is chosen as $\kappa = 0.41$ which seems to best fit the data at these Re_θ. Inspection of the log-law indicator function $\Xi = y^+(\mathrm{d}U^+/\mathrm{d}y^+)$, see Figure 4, shows that the current LES velocity profiles closely follow the composite profile proposed by Monkewitz *et al.* (2007) up to $y^+ \approx \mathcal{O}(100)$. Note that Ξ essentially measures the (inverse) von Kármán constant κ. The minimum of Ξ is reached at $y^+ \approx 70$ with a value of $1/\Xi \approx 0.428$ in good agreement with Monkewitz *et al.* (2007). The higher the Reynolds number, the longer the present LES data follows the composite profile, including the decreasing κ (increasing Ξ) after the minimum at $y^+ \approx 70$. However, even $Re_\theta = 4300$ is too low to reach an asymptotical logarithmic region (Österlund *et al.*, 1999) with the proposed $\kappa \approx 0.38$. In addition, it is interesting to note that in the inner region ($y^+ \approx 10$) the channel data

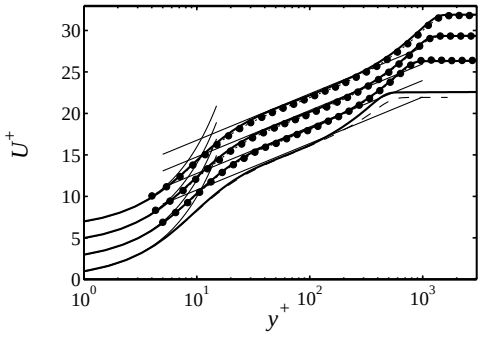

Figure 3: Mean velocity profile U^+ in viscous units for ——— present LES at $Re_\theta = 1430, 2558, 3661, 4303$, • measurements by Österlund (1999) at $Re_\theta = 2532, 3651, 4312$. – – – – DNS by Spalart (1988) at $Re_\theta = 1410$. The profiles are shifted by $U^+ = 2$ along the ordinate for increasing Re_θ. The linear and logarithmic regions are indicated by a thin line, using $1/\kappa \log y^+ + B$ with $\kappa = 0.41$ and $B = 5.2$.

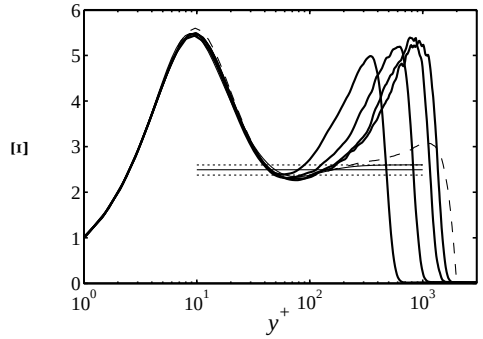

Figure 4: Indicator function $\Xi = y^+(\mathrm{d}U^+/\mathrm{d}y^+)$ for increasing $Re_\theta = 1430, 2558, 3661, 4303$. – – – – DNS of channel flow (Hoyas and Jiménez, 2006). The horizontal lines correspond to a von Kármán contant of $1/\kappa = 1/0.38$, $1/0.4$ and $1/0.42$, respectively.

by Hoyas and Jiménez (2006) features a slightly larger Ξ than the boundary-layer data. This behaviour is similar to a boundary layer under (weak) favourable pressure gradient (Schlatter and Brandt, 2008), which demonstrates the sensitivity of the near-wall region to possible pressure gradients as present in *e.g.* channel flow.

The velocity fluctuations, *e.g.* $u_{\mathrm{rms}} = \sqrt{\langle u'u' \rangle}$, and the Reynolds shear stress are depicted in Figure 5 in wall scaling, together with the total shear stress $-\langle u'v' \rangle + (1/Re)\mathrm{d}\langle U \rangle/\mathrm{d}y$. The agreement between the LES and a DNS at $Re_\theta = 2500$ is good (not shown). As mentioned in many studies, there is only incomplete collapse in inner scaling (see *e.g.* Hoyas and Jiménez (2006)), most dominantly for the streamwise and spanwise fluctuations. In particular, the maximum wall-normal value of u_{rms} is shown in Figure 6, clearly showing a Reynolds-number dependence, similarly as for the channel results. On the other hand, the total shear stress, scaled in outer units, appears to scale well for the considered range of Re_θ.

Based on the simulation results, the individual terms in the von Kármán integral equation relating the local skin friction to the growth of the momentum thickness θ may be considered, see Figure 7. It turns out that the term $U_\infty^2 \mathrm{d}\theta/\mathrm{d}x$ is $\mathcal{O}(50)$ times larger than the second relevant term, the integrated normal-stress difference. In addition, Figure 7 also provides a practical measure for the useful region of the simulation, *i.e.* the region in which an equilibrium turbulent boundary layer is recovered.

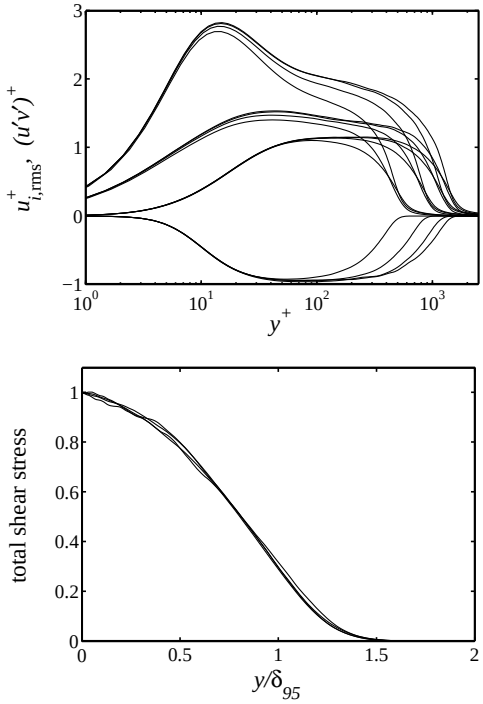

Figure 5: *Top:* Reynolds stresses for the present LES at $Re_\theta = 1430, 2558, 3661, 4303$. *Bottom:* Total shear stress in viscous scaling.

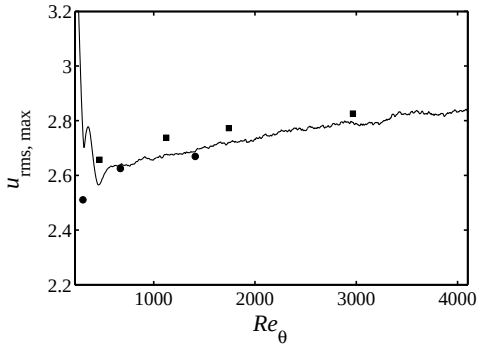

Figure 6: Wall-normal maximum of the streamwise fluctuations $u_{\mathrm{rms,max}}$ for ——— present LES, • DNS by Spalart (1988) and ■ DNS of channel flow (Moser *et al.*, 1999; del Álamo *et al.*, 2004).

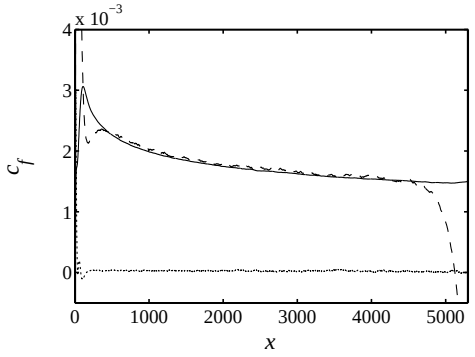

Figure 7: ——— Skin friction coefficient c_f compared to the individual terms of the von Kármán equation: ····· integral of the normal-stress difference, – – – – $U_\infty^2 \mathrm{d}\theta/\mathrm{d}x$.

In particular in the modelling community, there is considerable interest in data pertaining to the behaviour of the

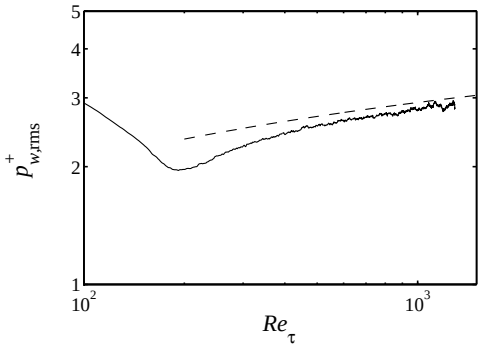

Figure 8: ——— Pressure fluctuations at the wall $p^+_{w,\mathrm{rms}}$ as a function of the friction Reynolds number Re_τ. - - - - $(p^+_{w,\mathrm{rms}})^2 = 6.5 + 1.86\log(Re_\tau/333)$ (Farabee and Casarella, 1991).

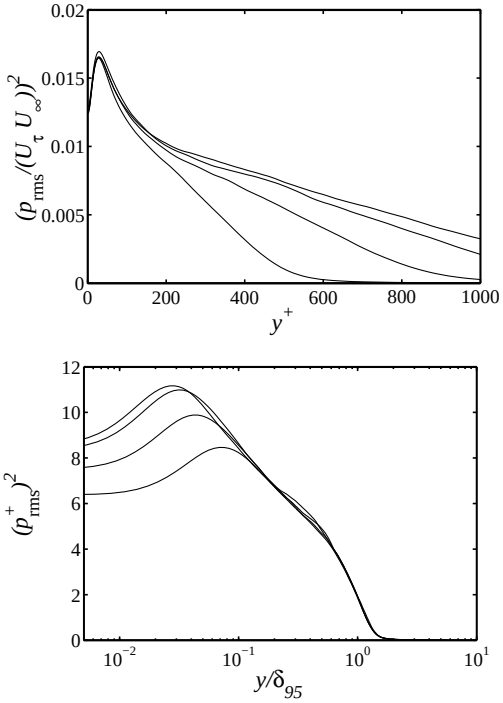

Figure 9: Wall-normal profiles of the pressure fluctuations for the present LES at $Re_\theta = 1430, 2558, 3661, 4303$.

pressure and its fluctuations throughout the boundary layer. Experimentally, it is very difficult to accurately measure the pressure (Tsuji *et al.*, 2007). In Figure 8 the wall pressure fluctuations are shown, and Figure 9 provides wall-normal profiles of p_{rms} with different scalings. As can be seen, a mixed scaling $p_{w,\mathrm{rms}}/(U_\tau \cdot U_\infty)$ is most appropriate close to the wall reaching approximately a value of 0.11 at $y = 0$. In pure inner scaling, a collapse of the data at various Re_θ can be seen for $y > 0.1\delta_{99}$. At the wall, p_{rms} is approximately 10% higher than the pressure fluctuations in channel flow at a corresponding $Re_\tau = U_\tau\delta/\nu$ with δ being the 99%-boundary-layer thickness or the channel-half width, respectively.

TURBULENT STRUCTURES

The most apparent turbulent structures close to solid walls are the turbulent streaks, described and characterised by many researchers, see *e.g.* Kline *et al.* (1967) and recently Lin *et al.* (2008). The spanwise organisation of the near-wall turbulence may be characterised by considering spanwise two-point correlations $R_{\alpha\alpha}$ of a turbulent quantity α. In Figure 10, the spanwise two-point correlations of the velocity components at $y^+ \approx 8$, and of the wall shear stress τ_w are shown. It can be observed that the behaviour of $R_{\tau\tau}$ and R_{uu} is very similar, featuring a first minimum at $\Delta z^+ \approx 60$. The two-point correlation of the wall-normal velocity component R_{vv} exhibits a strong minimum at $\Delta z \approx 25$ (Kim *et al.*, 1987), about at half the separation as for u. However, with increasing Re_θ the first minimum of R_{uu} weakens, and a second flat minimum appears at larger separation $\Delta z = \mathcal{O}(\delta_{99})$ (del Álamo *et al.*, 2004). These large-scale structures have received considerable interest over the last years, both experimentally (*e.g.* Hutchins and Marusic (2007)) and numerically (del Álamo and Jiménez, 2003). Figure 11 shows a map of $R_{\tau\tau}$ as a function of the Reynolds number Re_θ. Two minima can be discerned: The inner peak, corresponding to the near-wall streaks, can clearly be seen with a spacing of about 120 (local) wall units, as the first minimum of $R_{\tau\tau}$ at $2\Delta z^+ \approx 120$ (dashed line in Figure 11). However, a second peak (solid line) scaling as $2\Delta z \approx 0.85\delta_{99}$ is clearly visible in the two-point correlation for higher Re_θ, indicating the footprint of the large-scale structures onto the fluctuating wall-shear stress. For $Re_\theta < 1000$, the two peaks merge into one and no clear separation is present. However, for $Re_\theta > 1500$ two distinct peaks can be observed.

The influence of the Reynolds number on the scale separation between the small scale (inner) peak and the larger scale (outer) peak is demonstrated in Figure 12 with the help of premultiplied spanwise spectra $k_z\Phi_{uu}(\lambda_z)/u^2_{\mathrm{rms}}$ of the streamwise velocity u. The large-scale peak is clearly scaling in outer units, *i.e.* attaining its maximum at approximately at $y = 0.4\delta_{99}$ with a size $\lambda_z \approx 0.8\delta_{99}$. Scaling the energy spectra with U^2_τ (Figure 13), the outer peak reaches its maximum at a wall-normal distance of approximately $0.1\delta_{99}$ (Hutchins and Marusic, 2007). The inner peak is

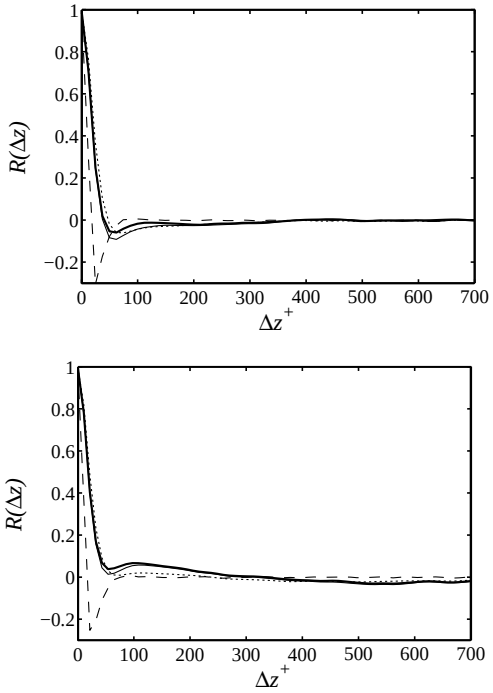

Figure 10: Spanwise two-point correlation $R_{\alpha\alpha}(\Delta z)$ for ——— streamwise velocity u, - - - - wall-normal velocity v, ····· spanwise velocity w (at $y^+ \approx 8$) and ——— the wall shear stress τ_w. *Top:* $Re_\theta = 1430$, *Bottom:* $Re_\theta = 4304$.

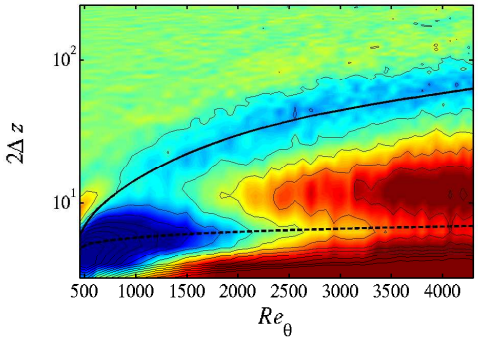

Figure 11: Spanwise two-point correlation $R_{\tau\tau}$ of the wall-shear stress τ_w computed from the present LES. The spanwise axis is scaled by the displacement $2\Delta z$ in order to directly show the spanwise pattern spacing. ——— corresponds to $0.85\delta_{99}$, - - - - corresponds to 120 plus units. The colors range from blue ($R_{\tau\tau} \leq -0.06$) to red ($R_{\tau\tau} \geq 0.06$); contour lines go from -0.15 to 0.15 with spacing 0.02.

consistently found at a wall-normal distance of $y^+ \approx 15$ (see *e.g.* del Álamo and Jiménez (2003)).

However, as opposed to channel flow, the definition of streamwise spectra and thus the streamwise size of the turbulent structures is not as obvious due to the spatial development of the flow. Usually, the Taylor hypothesis is invoked, assuming a certain convection velocity to transform temporal signals into spatial ones. In Figure 14, however, temporal spectra recorded at a number of probes located in the flow are presented for two Reynolds numbers. A fairly broad range of temporal frequencies is seen to be excited in the near-wall region ($y \approx 15$), and with higher Re a tendency towards larger (*i.e.* longer lasting) structures is seen in the outer region $y^+ > 100$. These structure have then an extent of $\mathcal{O}(6\delta_{99}/U_\infty)$. The present results are in agreement with the findings by Hutchins and Marusic (2007) and Jiménez and Hoyas (2008).

CONCLUSIONS

Well-resolved large-eddy simulations (LES) of a spatially developing turbulent boundary layer under zero pressure gradient up to relatively high Reynolds numbers ($Re_\theta = 4300$) are presented. The employed subgrid-scale model is ADM-RT, which is an efficient and simple regularisation based on high-order filters. The inflow is located at $Re_{\delta^*} = 450$ ($Re_\theta \approx 300$), a position upstream enough to ensure a proper flow development further downstream. Results are validated and compared extensively to both numerical data sets and available experimental measurements, *e.g.* the ones obtained by Österlund *et al.* (1999).

The goal of the present study is to provide reliable numerical data for high Reynolds-number wall-bounded turbulence, which can in turn be employed for further model development and validation, but also to contribute to the further characterisation and understanding of wall turbulence, in particular boundary-layer flows.

The LES results are in good agreement with existing data for both mean and fluctuating quantities, *e.g.* mean velocity, skin friction, and pressure fluctuations. In addition, spanwise and temporal spectra characterising large-scale flow organisation have been analysed. The present contribution focuses on presenting selected results, in an effort to validate the chosen simulation approach, and to initiate further studies analysing the simulation data.

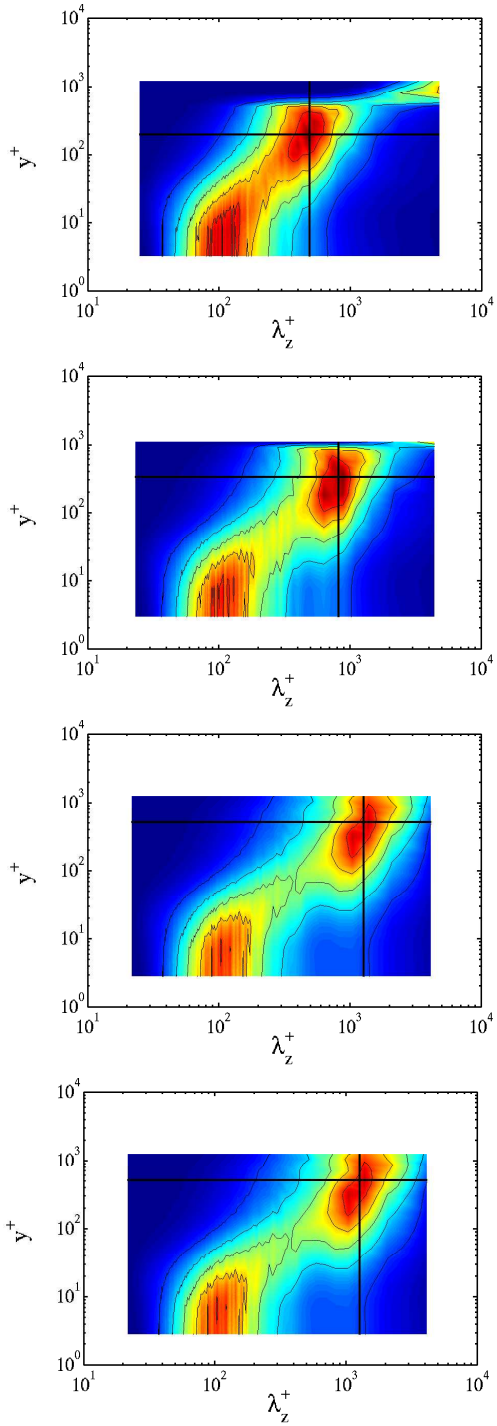

Figure 12: Premultiplied spanwise spectra $k_z\Phi_{uu}(\lambda_z)/u^2_{\rm rms}$ of the streamwise velocity fluctuation u. The vertical lines indicate $\lambda_z = 0.8\delta_{99}$, the horizontal lines $y = 0.4\delta_{99}$. From *top* till *bottom*: $Re_\theta = 1430, 2558, 3661, 4303$.

REFERENCES

del Álamo, J. C. and Jiménez, J., 2003. "Spectra of the very large anisotropic scales in turbulent channels." *Phys. Fluids*, vol. 15(6), pp. L41–L44.

del Álamo, J. C., Jiménez, J., Zandonade, P., and Moser, R. D., 2004. "Scaling of the energy spectra of turbulent channels." *J. Fluid Mech.*, vol. 500, pp. 135–144.

Chevalier, M., Schlatter, P., Lundbladh, A., and Henningson, D. S., 2007. "SIMSON - A Pseudo-Spectral Solver for Incompressible Boundary Layer Flows." Tech. Rep.

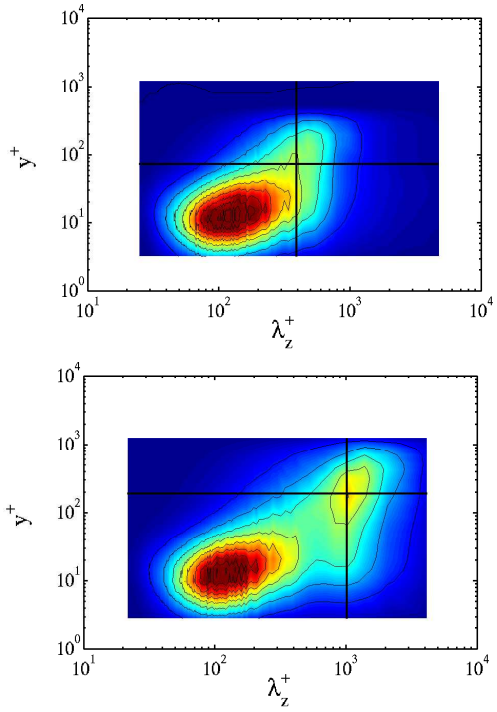

Figure 13: Premultiplied spanwise spectra $k_z\Phi_{uu}(\lambda_z)/U_\tau^2$ of the streamwise velocity fluctuation u. The vertical lines indicate $\lambda_z = 0.8\delta_{99}$, the horizontal lines $y = 0.1\delta_{99}$. *Top*: $Re_\theta = 1430$, *bottom*: $Re_\theta = 4303$.

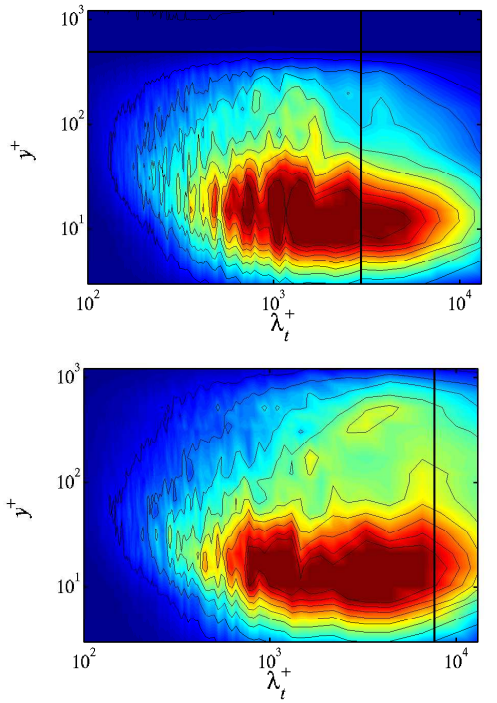

Figure 14: Premultiplied temporal spectrum $\omega\Phi_{uu}(\lambda_t)/U_\tau^2$ of the streamwise velocity fluctuation u. The vertical lines indicate $\lambda_t = 6\delta_{99}/U_\infty$, the horizontal lines $y = \delta_{99}$. *Top*: $Re_\theta = 1430$, *bottom*: $Re_\theta = 4303$.

TRITA-MEK 2007:07, KTH Mechanics, Stockholm, Sweden.

Farabee, T. M. and Casarella, M. J., 1991. "Spectral features of wall pressure fluctuations beneath turbulent boundary layers." *Phys. Fluids*, vol. 3, pp. 2410–2420.

Ferrante, A. and Elghobashi, S., 2005. "Rreynolds number effect on drag reduction in a microbubble-laden spatially developing turbulent boundary layer." *J. Fluid Mech.*, vol. 543, pp. 93–106.

Honkan, A. and Andreopoulos, Y., 1997. "Vorticity, strain-rate and dissipation characteristics in the near-wall region of turbulent boundary layers." *J. Fluid Mech.*, vol. 350, pp. 29–96.

Hoyas, S. and Jiménez, J., 2006. "Scaling of the velocity fluctuations in turbulent channels up to $Re_\tau = 2003$." *Phys. Fluids*, vol. 18(011702), pp. 1–4.

Hutchins, N. and Marusic, I., 2007. "Evidence of very long meandering features in the logarithmic region of turbulent boundary layers." *J. Fluid Mech.*, vol. 579, pp. 1–28.

Jiménez, J. and Hoyas, S., 2008. "Turbulent fluctuations above the buffer layer of wall-bounded flows." *J. Fluid Mech.*, vol. 611, pp. 215–236.

Kays, W. M. and Crawford, M. E., 1993. *Convective Heat and Mass Transfer*. McGraw-Hill, New York, U.S.A., 3rd ed.

Khujadze, G. and Oberlack, M., 2004. "DNS and scaling laws from new symmetry groups of ZPG turbulent boundary layer flow." *Theoret. Comput. Fluid Dynamics*, vol. 18, pp. 391–411.

Kim, J., Moin, P., and Moser, R., 1987. "Turbulence statistics in fully developed channel flow at low Reynolds number." *J. Fluid Mech.*, vol. 177, pp. 133–166.

Kline, S. J., Reynolds, W. C., Schraub, F. A., and Runstadler, P. W., 1967. "The structure of turbulent boundary layers." *J. Fluid Mech.*, vol. 30, pp. 741–773.

Komminaho, J. and Skote, M., 2002. "Reynolds stress budgets in Couette and boundary layer flows." *Flow Turbulence Combust.*, vol. 68(2), pp. 167–192.

Lin, J., Laval, J. P., Foucaut, J. M., and Stanislas, M., 2008. "Quantitative characterization of coherent structures in the buffer layer of near-wall turbulence. part 1: streaks." *Exp. Fluids*, vol. 45, pp. 999–1013.

Monkewitz, P. A., Chauhan, K. A., and Nagib, H. M., 2007. "Self-consistent high-Reynolds-number asymptotics for zero-pressure-gradient turbulent boundary layers." *Phys. Fluids*, vol. 19(115101), pp. 1–12.

Moser, R. D., Kim, J., and Mansour, N. N., 1999. "Direct numerical simulation of turbulent channel flow up to $Re_\tau = 590$." *Phys. Fluids*, vol. 11(4), pp. 943–945.

Österlund, J. M., 1999. *Experimental studies of zero pressure-gradient turbulent boundary-layer flow*. Ph.D. thesis, Department of Mechanics, KTH Stockholm, Sweden.

Österlund, J. M., Johansson, A. V., Nagib, H. M., and Hites, M. H., 1999. "A note on the overlap region in turbulent boundary layers." *Phys. Fluids*, vol. 12(1), pp. 1–4.

Schlatter, P. and Brandt, L., 2008. "DNS of three-dimensional turbulent boundary layers." In *Direct and Large-Eddy Simulation 7, September 8-10*. To appear.

Schlatter, P., Stolz, S., and Kleiser, L., 2004. "LES of transitional flows using the approximate deconvolution model." *Int. J. Heat Fluid Flow*, vol. 25(3), pp. 549–558.

Schlatter, P., Stolz, S., and Kleiser, L., 2006. "LES of spatial transition in plane channel flow." *J. Turbulence*, vol. 7(33), pp. 1–24.

Spalart, P. R., 1988. "Direct simulation of a turbulent boundary layer up to $R_\theta = 1410$." *J. Fluid Mech.*, vol. 187, pp. 61–98.

Tsuji, Y., Fransson, J. H. M., Alfredsson, P. H., and Johansson, A. V., 2007. "Pressure statistics and their scaling in high-Reynolds-number turbulent boundary layer." *J. Fluid Mech.*, vol. 585, pp. 1–40.